Identification and monitoring of waterlogged areas in a productive region of Argentina using Landsat information
Lucía María Cappelletti, Anthony Schrapffer, Anna Sörensson
Meteorologica, 47(2), e014, julio-diciembre 2022
ISSN 1850-468X — https://doi.org/10.24215/1850468Xe014
http://www.meteorologica.org.ar
Centro Argentino de Meteorólogos
Buenos Aires — Argentina

IDENTIFICACION Y MONITOREO DE ÁREAS ANEGADAS EN UNA REGIÓN PRODUCTIVA DE ARGENTINA EMPLEANDO ESCENAS LANDSAT

Lucía María Cappelletti[1,2,3], Anthony Schrapffer[1,2,3], Anna Sörensson[1,2,3]

[1]Universidad de Buenos Aires, Facultad de Ciencias Exactas y Naturales. Buenos Aires, Argentina.
[2]CONICET – Universidad de Buenos Aires. Centro de Investigaciones del Mar y la Atmósfera (CIMA). Buenos Aires, Argentina.
[3]CNRS – IRD – CONICET – UBA. Instituto Franco-Argentino para el Estudio del Clima y sus Impactos (UMI 3351 IFAECI). Buenos Aires, Argentina.

(Manuscrito recibido el 5 de julio de 2021, en su versión final el 12 de octubre de 2021)

RESUMEN

El seguimiento de las zonas inundadas y anegadas es esencial para las pampas argentinas, una extensa región llana de gran productividad agrícola, ganadera e industrial. Áreas dentro de las pampas han experimentado un aumento del nivel freático en los últimos años, un factor clave que contribuye al desarrollo y la persistencia de las inundaciones. El monitoreo de estos fenómenos ambientales extremos es esencial tanto para objetivos a largo plazo, como aumentar el conocimiento de los mismos para poder modelar y predecir su evolución, como para objetivos prácticos a corto plazo, como la planificación efectiva del uso del suelo durante un evento en curso. Por lo tanto, el objetivo principal de este trabajo es desarrollar un método sencillo para el seguimiento de las zonas afectadas, utilizando herramientas accesibles. Se eligió como sitio de estudio una región de 160 km^2 del sudeste de Córdoba, de la cual se dispone de datos de altura de nivel freático y de precipitación diaria. Para determinar las zonas inundadas del lugar, se utilizaron 18 imágenes Landsat-8/OLI entre septiembre de 2019 y abril de 2021. En cada una de estas imágenes, los píxeles se etiquetan según tres categorías: Agua Abierta, Agua-Mixta y No-Agua aplicando un método de clasificación no supervisada de los índices de agua mNDWI y NDWI. A pesar de la falta de escenas debido a la cobertura de nubes y sus sombras que pueden sufrir las escenas, la categoría de Agua Abierta, y en menor grado la categoría Agua-Mixta, son capaces de captar los cambios en la altura del nivel freático debido a precipitaciones.
Palabras clave: Monitoreo de Inundaciones y Anegamientos, Identificación de Agua Superficial, Índices Espectrales, Data Geoespacial, Sensores Remotos.

IDENTIFICATION AND MONITORING OF WATERLOGGED AREAS IN A PRODUCTIVE REGION OF ARGENTINA USING LANDSAT INFORMATION

ABSTRACT

The monitoring of flooded and waterlogged areas is essential for the Argentinean Pampas, an extensive flat region of high agricultural, livestock and industrial productivity. Areas within the Argentinean Pampas have experienced a rise of

Dirección Electrónica: lucia.cappelletti@cima.fcen.uba.ar

the water table in recent years, a key factor contributing to the development and persistence of flooding. The monitoring of these extreme environmental events is essential for long-term objectives, e.g. increasing knowledge to model and predict the occurrence and evolution of extreme events; as well as for short-term objectives, e.g. to provide producers potential field management options in a flood emergency. Therefore, the main objective of this work is to develop a simple method for monitoring affected areas, using accessible tools. A 160 km^2 region of southeastern Córdoba for which data on water table height and daily precipitation are available, was chosen as a study site. To determine the flooded areas of the site, 18 Landsat-8/OLI images from September 2019 - April 2021 were used. On each of these images, pixels were labeled according to three categories: Open Water, Mixed-Water and Non-Water by applying unsupervised classification of the mNDWI and NDWI water indices. Despite the lack of scenes due to cloud cover the scenes may suffer, the Open Water category, and to a lower degree the Mixed-Water category, are able to capture the changes in the water table height due to precipitation.
Keywords: Flood and Waterlogging Monitoring, Surface Water Identification, Spectral Indices, Geospatial Data, Remote Sensing.

1. INTRODUCCIÓN

The Argentinean Pampas is an extensive plain of approximately 500,000 km^2, with rainfall of 600-1200 $mm^1 year^{-1}$ and less than 1 % slope (Kruse and Zimmermann, 2002) and is a core region of agricultural, livestock and industrial productivity. Areas within the Pampas, such as the southern and central part of the province of Córdoba, have recorded rising water tables in several places due to the extensive land use and management change (Bollatti et al., 2016). These characteristics make the region prone to waterlogging and flooding. The combination of these extreme hydrological events and intensive land use create a disharmonious combination between ecosystem conservation, efficient agricultural practices and human well-being (Nosetto et al., 2009; Viglizzo et al., 2009). In the presence of this problem, effective land-use planning needs to be implemented, and to this end it is essential to increase understanding of the causes and dynamics of these extreme environmental events by developing tools for monitoring affected areas.

Satellites equipped with multispectral instruments are able to detect surface features on a global scale, exploiting the spectral absorption or emission characteristics of objects. For example, since 1972, multispectral information from Landsat satellites has made it possible to track and document land changes due to land use, forest fires and floods, among other natural and human-induced changes (U.S. Geological Survey, 2016). One of the ways to make use of this type of information is through the development of indices to highlight different features (e.g., Oleksiak 2008; Ma et al., 2020). As the element to be studied is surface water, we are interested in indices that allow us to highlight them. In this sense, for example, McFeeters (1996) developed the Normalized Difference Water Index (NDWI) using the green and near-infrared (NIR) bands. Its function is to differentiate water from other elements, taking into account that water absorbs the incident radiant flux almost entirely in the near- and shortwave- infrared bands, while the land surface reflects a significant amount of energy in this range of the electromagnetic spectrum. In contrast, the incorporation of the green band maximizes the reflectance of the

water. This index is given by:

$$NDWI = \frac{Green - NIR}{Green + NIR} \quad (1)$$

For the use of NDWI, with values between -1 and 1, McFeeters (1996) proposed the use of its positive values to identify water bodies and negative values for non-water features, but it has limitations in suppressing built-up areas. Xu (2006) proposed the modified Normalised Difference Water Index (mNDWI), in which the NIR band is replaced by the shortwave - infrared (SWIR) band. The mNDWI has been shown to be more effective in distinguishing water from built-up areas. The expression of this index, also with values between -1 and 1, is:

$$mNDWI = \frac{Green - SWIR}{Green + SWIR} \quad (2)$$

Here we present a method for monitoring flooded areas based on the above indices. These were computed using multispectral data from the Landsat 8 satellite system, launched in 2013 and developed as a collaboration between the National Aeronautics and Space Administration (NASA) and the U.S. Geological Survey (USGS). Previous studies such as Pasucci (2017); and Ferral et al. (2019), use Landsat 8 scenes and spectral indices for the identification of flooded and non-flooded areas of sites in the Argentinean Pampas. In this work, were used and combined the NDWI and mNDWI to label each pixel of the area according to the amount of surface water it contains. The pixels were grouped into three different categories: Non-Water, Mixed-Water and Open Water. The decomposition in these three groups is a delicate task due to the interplay of different factors, such as the presence of vegetation and its large seasonal variability but also the division of the year in a dry and wet season which may impact the land properties (Li et al., 2015). For these reasons, we decided to classify the pixels using an unsupervised classification method, as it is simple to implement and widely used in remote sensing applications (e.g., Boschetti et al., 2014). A 160 km^2 area was selected as a study site in the south-eastern centre of the province of Córdoba, where waterlogging and flooding have the water table as one of their key elements.

The flood detection algorithm was run on Landsat 8 images of dry seasons as well as on dates of flood events reported by Argentinean institutions, such as the National Institute of Agricultural Technology (INTA for its spanish acronym), in order to take into account the hydrological dynamics of the region and obtain a single threshold per pixel category.

2. METHODS AND MATERIALS

2.1. Study area

The study region is located in the proximity of Justiniano Posse, a location in the east of Córdoba Province, Argentina (Figure 1). It has wet summers (mean 4.2 mm^1day^{-1}) with maximum temperatures reaching 31 °C in January, and drier winters (¡1 mm^1day^{-1}) with minimum temperatures of 4 °C in July (National Meteorological Service. `https://www.smn.gob.ar/estadisticas`, accessed on 25 August 2021). The selected area, approximately 160 km^2, is part of a region of high agricultural productivity of annual crops and pastures managed without irrigation (IDECOR. `https://idecor.cba.gov.ar`, accessed on 25 August 2021), characterized by a plain of normal relief with numerous relatively small areas of subnormal - concave relief, which give rise to ponds (Capdevila et al., 2016).

2.2. In Situ and Satellite Data

Since rainfall and water table height variation in the region of interest are critical factors in the occurrence and duration of waterlogging and flooding, in situ data of these variables was used to evaluate the performance of the method we developed. In the region of study, data from one in situ sensor located in Justiniano Posse was available (data was provided by the Rural Extension Agency of INTA Justiniano Posse). The availability of in situ data limited the study

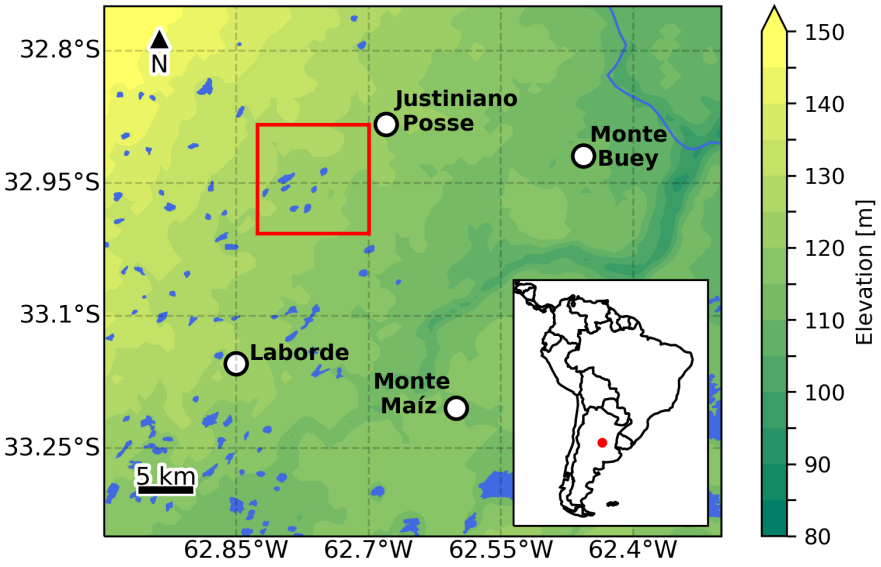

Figure 1: Topographic map (m) of the study site (red square in the regional map); and the water bodies present (Source: National Geographic Institute of the Argentine Republic, IGN. https://www.ign.gob.ar/, accessed on 25 August 2021). The region is located in the Province of Córdoba, Argentina (red dot in the map of South America).

period to September 2019 - April 2021.

In order to implement the flood monitoring tool over the Justiniano Posse region, Landsat 8 images corresponding to path 228 and row 083 were used. The scene set was acquired through the USGS Earth Explorer (U.S. Geological Survey, `https://earthexplorer.usgs.gov`, accessed on 25 August 2021). The Landsat 8 satellite carries the Operational Land Imager (OLI) which collects image data for nine spectral bands. As detailed in Table I, the sensor provides scenes with a spatial resolution of 30 m (visible, NIR, SWIR bands), and 15 m (panchromatic band). The scenes used correspond to the Level 2 Surface Reflectance product, which is derived from the top of atmosphere reflectance product (Level 1) that has been corrected for the temporally, spatially and spectrally varying scattering and absorbing effects of atmospheric gases, aerosols, and water vapor (Vermote et al., 2016). Within this processing level, the USGS recommends using information from Collection 2 (U.S. Geological Survey, `https://www.usgs.gov/core-science-systems/nli/landsat`, accessed on 25 August 2021). The cloud cover present in the satellite optical products poses a challenge for flood detection. To avoid contamination of the images by cirrus, clouds and their shadows; the scenes have been filtered in two steps: (1) using the cloud cover score "Scene Cloud Cover" listed in the EarthExplorer metadata, we select the scenes with a score lower than 5 %, which is a reasonable value following Acharya et al. (2018). The Scene Cloud Cover score is determined by the C Function of Mask algorithm, that provides an estimation of the percentage of cloud cover calculated over an entire Landsat scene (Foga et al., 2017) and (2) filtering manually these scenes as recommended by Ferral et al. (2019). This filtering applied over the corresponding study period resulted in 18 images that can be analysed (Table II).

2.3. Methods: Detection of the Water Cover of Scenes

Both NDWI and mNDWI were used since they are useful for the detection of clear water. An approach combining the two

Satellite	Sensor Band	Name Wavelength [μm]	Resolution [m]
Landsat 8 - OLI	1 - Coastal Aerosol	0.43 - 0.45	30
	2 - Blue	0.45 - 0.51	30
	3 - Green	0.53 - 0.59	30
	4 - Red	0.64 - 0.67	30
	5 - Near - Infrared (NIR)	0.85 - 0.88	30
	6 - Shortwave - IR 1 (SWIR1)	1.57- 1.65	30
	7 - Shortwave - IR 2 (SWIR2)	2.11 - 2.29	30
	8 - Panchromatic	0.50 - 0.68	15
	9 - Cirrus	1.36 - 1.38	30

Table I: Landsat 8 Satellite - OLI sensor specifications.

	Scene's dates
Landsat 8 - OLI Collection 2 - Level 2 Path 228 / Row 083	2019-09-01
	2019-09-17
	2019-11-20
	2020-01-07
	2020-02-24
	2020-05-14
	2020-06-15
	2020-08-02
	2020-08-18
	2020-09-19
	2020-10-05
	2020-11-22
	2020-12-08
	2021-01-09
	2021-02-26
	2021-03-30
	2021-04-15
	2021-05-01

Table II: Specifications and dates of the scenes used.

indices was developed because the NDWI is sensitive to conditions of mixture of water and soil/vegetation and the mNDWI to water conditions in urban environments (Zhou et al., 2017). With this choice, we were able to identify and map flooded and waterlogged areas by three categories, in the following called Non-Water, Mixed-Water and Open Water. The Non-Water category refers to pixels with low to no water content, while Mixed-Water refers to pixels composed by soil/vegetation with a given percentage of water. The third category refers to permanent type water bodies, such as ponds.

The standard threshold for clear water areas in the case of both indices is values greater than 0. However, categorising the pixels according to the three labels mentioned above groups by optimal thresholds is a delicate task. In order to show the behaviour of the indices and the sensitivity of the thresholds, the NDWI and mNDWI indices were mapped for one wet scene (7 January 2020) and one dry scene (9 January 2021). In the dry scene, the preceding weather condition was close to the average, without any extreme rainfall events, while in the wet scene, both local media and the Crop Market of the Province of Córdoba (BCCBA. `https:`

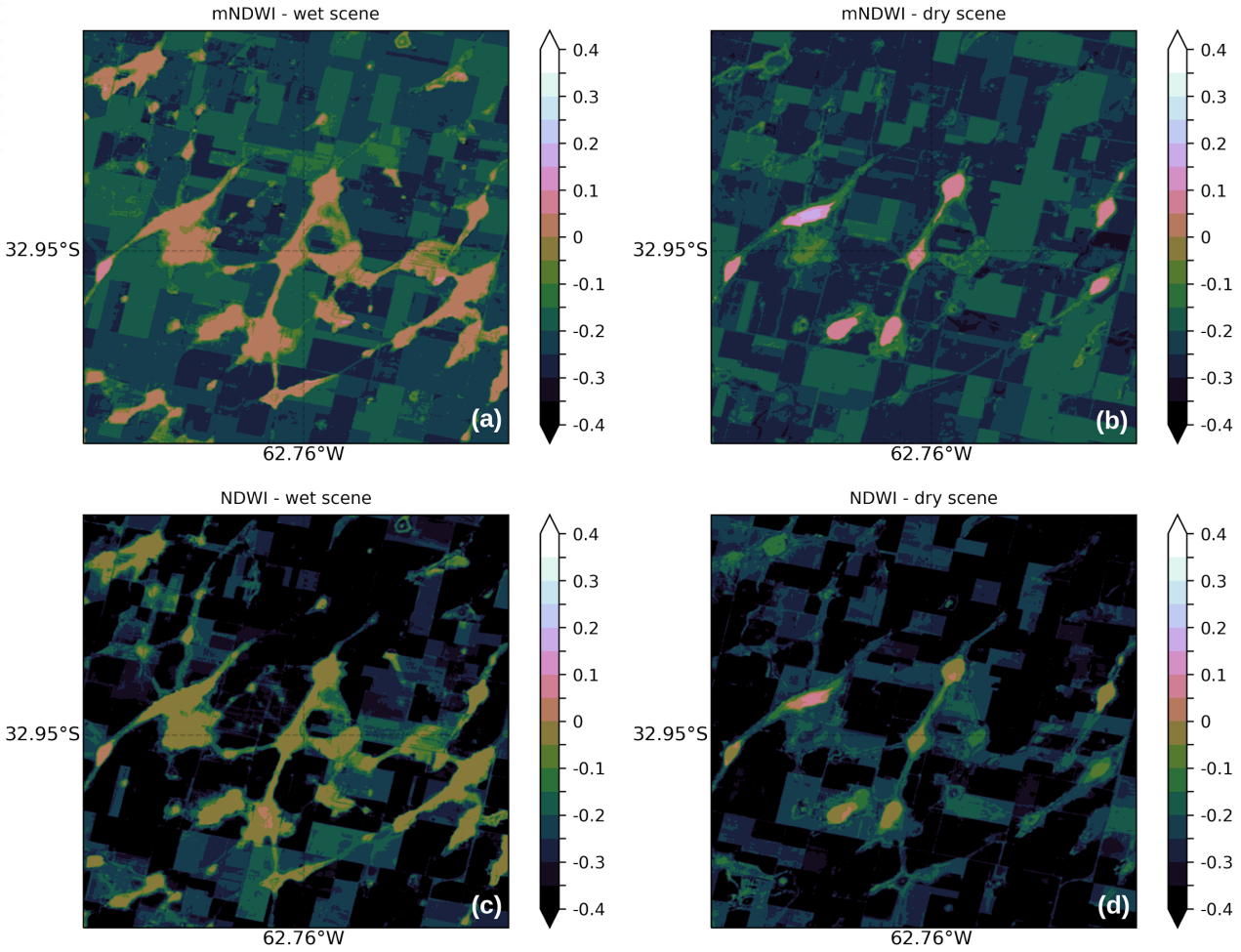

Figure 2: Mapping of the mNDWI and NDWI indices over the study site, based on Landsat 8 scenes from 7 January 2020 (wet scene) and 9 January 2021 (dry scene). (a): mNDWI, wet scene. (b): mNDWI, dry scene. (c): NDWI, wet scene. (d): NDWI, dry scene.

`//www.bccba.org.ar`, accessed on 25 August 2021) reported that Justiniano Posse, along with other neighbouring cities, suffered severe flooding at the beginning of January. In Figure 2 it can be noticed that both mNDWI and NDWI show analogous patterns in the differentiation of the wet scene from the dry. Using real colour images (RGB: B4-B3-B2 for Landsat 8) and the spectral signatures on pixel samples of both scenes (not shown) we noticed that, for the pixels corresponding to clear water, they presented positive mNDWI values. In the case of NDWI, the values of these same pixels, in general, resulted to be negative. Also, some pixels identified as clear water on both dates, through visual exploration and spectral signatures, have different values of NDWI and mNDWI; even though the two scenes are from the same period of the year. This is due to the fact that the thresholds are sensitive to different factors and their interplay, such as the year-to-year variability of soil water content and vegetation (Acharya et al., 2018).

The above example shows that obtaining optimal thresholds is a complex task, even in regions such as the one studied in this work, where there are no shadows generated by mountainous terrain. For clustering the pixels we used an unsupervised classification

method. We decided to use the traditional K-Means method, widely used for land cover classification based on remotely sensed data (e.g., Ogilvie et al., 2015) and easy to implement, using scikit-learn (Pedregosa et al., 2011), a Python library. The K-Means algorithm is well adaptable to a large number of samples and requires the number of clusters to be specified by the user.

The mNDWI and NDWI indices were calculated for the pixels of the 18 images, resulting in about 3,200,000 pixels labelled according to two variables each. On these pixels the K-Means method was applied using 10 clusters. Out of these 10 clusters only two contained pixels with positive values of both mNDWI and NDWI. The group with pixels with higher values for both indices (hereafter, cluster A) contains 94,542 pixels, of which 95 % have mNDWI ¿0, but in the case of NDWI, less than 40 % of the pixels have positive values. This behaviour of the same pixel presenting values of mNDWI >0 and NDWI < 0 was already noticed in the Figure 2. The other cluster that also has positive values for both indices (B) contains 59,449 pixels, of which 5 % refer to mNDWI > 0 and in the case of NDWI less than 1 % are positive. The remaining 8 clusters (grouped as cluster C) are composed entirely of pixels with negative mNDWI and NDWI values (Figure 3). Thus, we used class A to identify Open-Water pixels, B for Mixed-Water and C for the Non-Water label. To define the threshold representing each water condition label, in the case of Open Water we took the 0.05 quantile as its lower limit (90 % of class A). As for class B, approximately 94 % were below the lower limit of class A, thus for Mixed-Water it was decided to use the same limit as the upper limit, and the lower limit corresponding to the 0.05 quantile of class B (Mixed-Water is given by 80 % of class B). As for class B, approximately 94 % were below the lower limit of class A, thus for Mixed-Water it was decided to use the same limit as the upper limit, and the lower limit corresponding to the 0.05 quantile of class B (Mixed-Water is given by 80 % of class B). The other pixels that did not correspond to these conditions (class C) were treated as Non-Water. Table III shows the thresholds of the labels of interest to be used in the identification of Open Water and Mixed-Water areas.

3. RESULTS AND DISCUSSION

The area of Open Water and Mixed-Water was calculated using the thresholds shown in Table III. Figure 4 shows the time series of the precipitation corresponding to 5 day moving sum window daily (4a), water table height, from Justiniano Posse's in situ measurements (4b) as well as the number of pixels belonging to Open Water and Mixed-Water (4c). In Figure 4 it is noted that in January and mid-February of 2020 the water table height experiences two increases that are not noticeable in the Open and Mixed-Water areas; this is due to the lack of imagery in that period. The next closest scene is 2020-02-24, at which time the water table decreased in height to around -150 cm since its last notable rise in mid-February.

From April to mid-October 2020, the water table height decreases from -100 cm to approximately -175 cm, with a mean decrease rate of 1.4 cm between days. This stabilisation of the water table height is reflected in the behaviour of the Open Water area; whereas the Mixed-Water area peaks in 2020-09-19, despite the fact that no precipitation was registered in previous days.

Concerning the final months of 2020, 2020-10-25 and 2020-12-18, the water table height rise by approximately 30 cm in two days due to accumulated rainfall above 50 mm. As for the October date, it is possible to notice a slight increase of 870 Open Water pixels between the available scenes of 2020-10-05 and 2020-11-22. At the end of January 2021, on the 2021-01-28 and 2021-01-29, the precipitation exceeded 60 mm and 80 mm respectively, which resulted in an increase of the water table from -228 cm to -72 cm in only two days. In the case of such an event, a notable increase in the area of Open Water and Mixed-Water was expected,

Water Condition	Threshold
Open Water	MNDWI > 0 and NDWI > -0.09
Mixed-Water	0 > mNDWI > -0.15 and -0.09 > NDWI > -0.19

Table III: Ranges of values of the mNDWI and NDWI indices established to detect pixels corresponding to the Open Water and Mixed-Water categories.

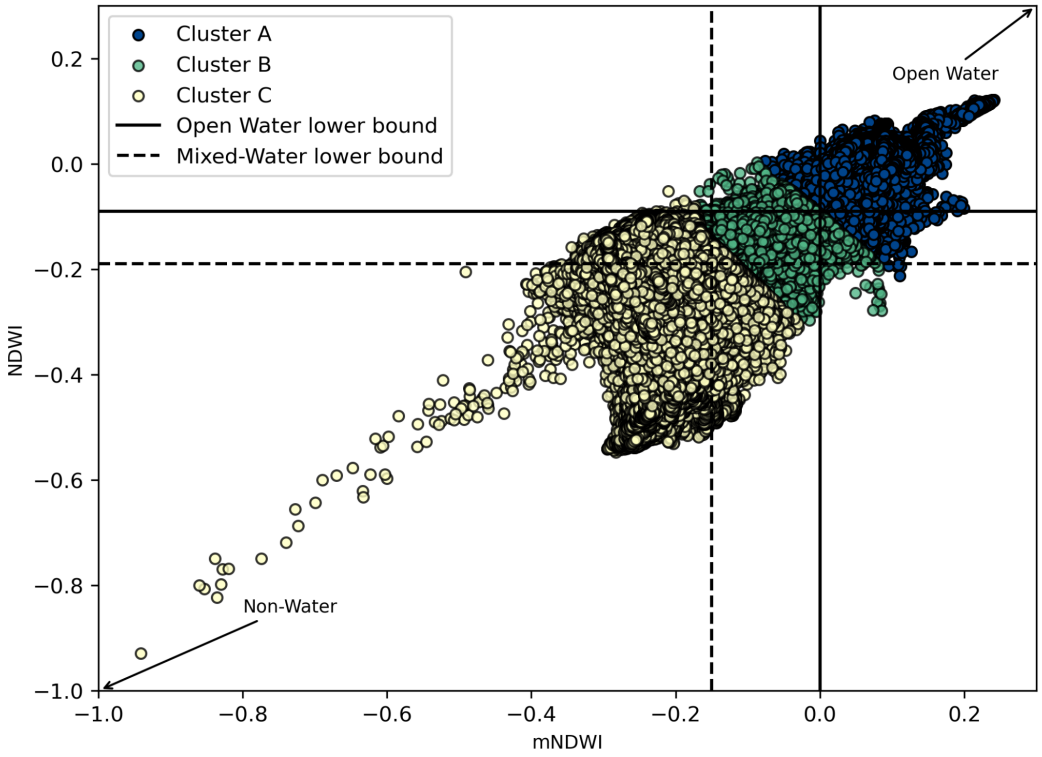

Figure 3: Scatterplot of the pixels of the 18 images analysed in this study according to their mNDWI and NDWI values. The colours identify to which cluster each pixel belongs, according to the unsupervised KMeans classification method and subsequent grouping: cluster A, cluster B and cluster C. Also, the lower bounds of the thresholds referring to Open Water (solid line) and Mixed-Water (dashed line) are plotted.

due to the response of these variables to the similar situation at the beginning of January 2020. Although the rainfall conditions in the summers of 2020 and 2021 are similar, the Open Water area is notably different. This is explained by the the fact that in 2020, the difference in days between the extreme precipitation event and the available Landsat scene is 4 days (rainfall: 2020-01-03, available Landsat scene: 2020-01-07), while in 2021 it is 24 days (rainfall: 2021-02-02, available Landsat scene: 2021-02-26). This example showcases the difficulty imposed by the low availability of images, in particular during the summer season since more images are discarded due to cloudiness.

As a graphical example of Open Water and Mixed-Water detection, the categories were mapped onto the dry scene and wet

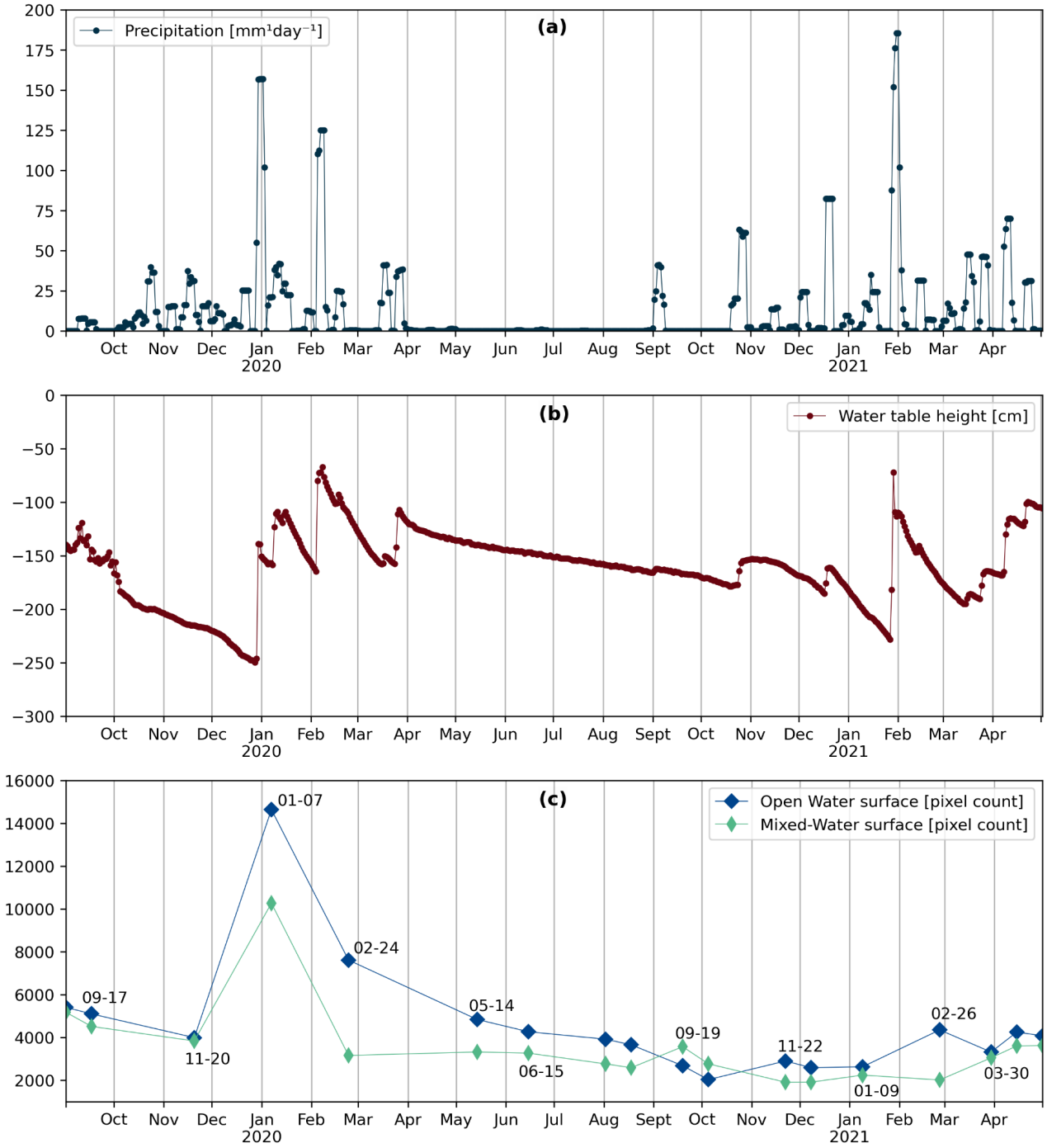

Figure 4: Time series of (a): precipitation corresponding to 5 day moving sum window [$mm^1 day^{-1}$], i.e., the value of a certain day is the sum of the daily precipitation of that day added to those corresponding to 4 previous days, (b): daily water table height in reference to the terrain level [cm]. The daily precipitation and water table height data refer to in situ measurements at Justiniano Posse (INTA Justiniano Posse). (c): number of pixels classified as Open Water and Mixed-Water, according to the thresholds in Table III. Some of the amounts are shown together with the date of the corresponding scene.

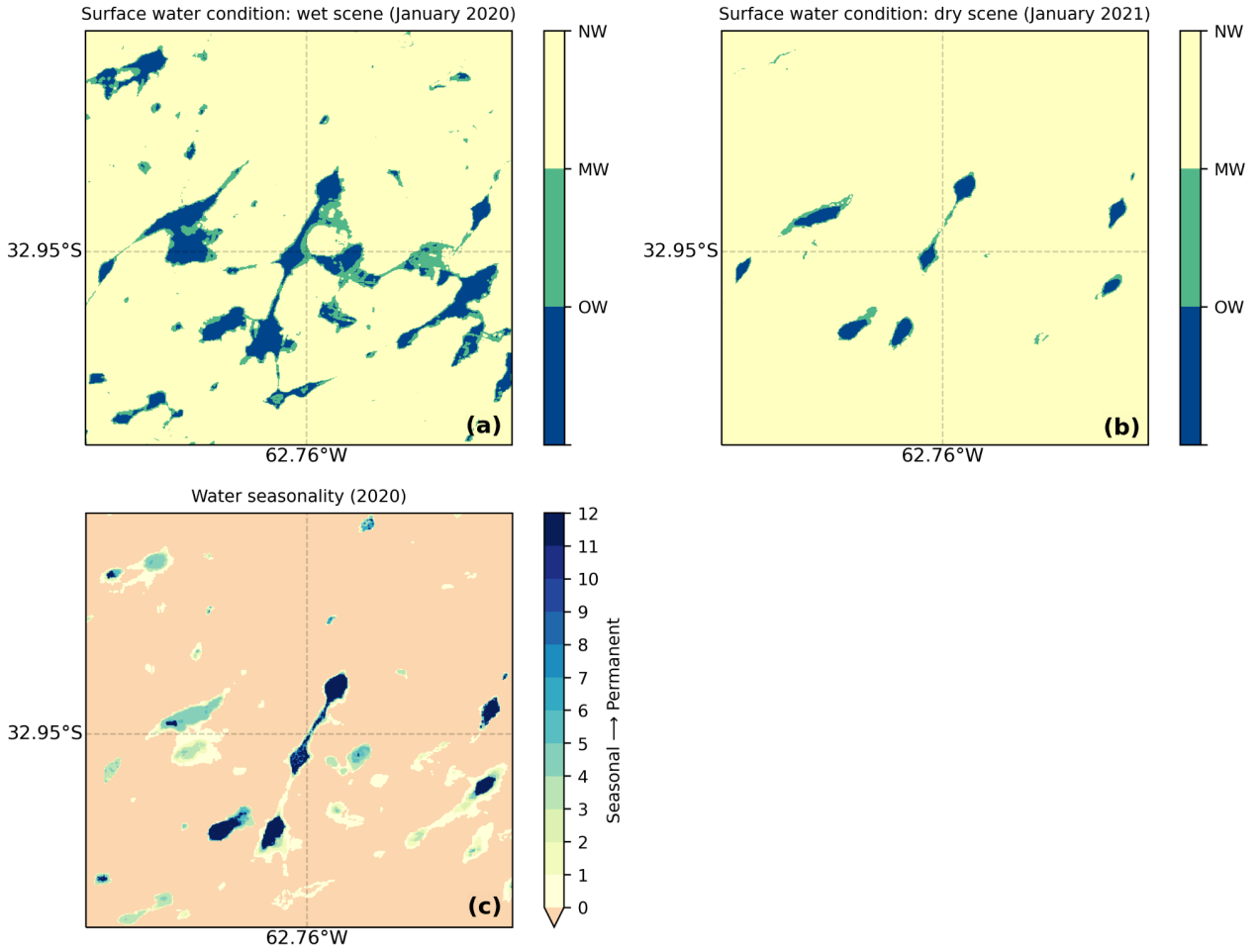

Figure 5: Mapping of Open Water (OW), Mixed-Water (MW) and Non-Water (NW) condition categories over the study site, based on Landsat 8 scenes from 7 January 2020 (wet scene), in panel (a) and 9 January 2021 (dry scene), in (b). Pixels were labelled according to the thresholds set out in Table III. In (c) the Water Seasonality product for the year 2020 (Source: EC JRC/Google) is shown over the same region. Permanent water is shown in dark blue and seasonal water areas are shown in blue with increased white contribution. Data were scaled from 1 month to 12 months for each year, a value of 0 represents zero contribution of the Water Seasonality product.

scene, introduced earlier. Both results were contrasted with information from the monthly and 30 m resolution water maps provided by the Joint Research Center (JRC) of the European Commission (EC), developed from Landsat images (Pekel et al., 2016). This database offers several products, for our study we were interested in using the Water Seasonality 2020 (`https://global-surface-water.appspot.com/map`, accessed on 25 August 2021). The Water Seasonality product provides information concerning the intra-annual behaviour of water bodies. It separates "permanent" water bodies (those that are present during the whole observation period, in this case 2020) from "seasonal" water bodies (those that are present only during a part of the year); the degree of seasonality is represented by the proportion of the total number of months (from 1 to 12) in which water is present. Figure 5 shows these three mappings. Pixels that belong to Open

Water in the dry scene are also Open Water in the wet scene. As for the JRC EC product, all pixels that refer to permanent water, i.e. they have water 12 months of the year, are Open Water in the wet scene. Regarding the Water Seasonality pixels less than 12 months, most of them refer to Open Water in the wet scene and less to Mixed-Water.

For the example shown, it was more difficult to contrast the information from the Mixed-Water category than the Open Water category. In addition, through the analysis of time series, it was possible to appreciate that Mixed-Water shows a reduced degree of change in relation to fluctuations in the water table, in response to rainfall. In the study conducted by Ferral et al. (2019) it is explained that the Mixed-Water category is more difficult to contrast, as the accurate delineation of pond shorelines or the determination of mixed pixels, composed of soil/vegetation with a certain percentage of water, is difficult to deal with when using data from a single sensor. Additionally, it is worth noting that the use of more than one sensor would help to avoid information gaps due to, for example, image filtering due to cloud cover, a limiting factor in our work.

4. CONCLUSION

We calculated the mNDWI and NDWI water indices of 18 Landsat 8 images, from September 2019 - April 2021, and selected the thresholds to define the Open Water and Mixed-Water categories by applying an unsupervised classification method. We found that the number of pure water pixels and mixed water pixels, i.e. vegetation/soil with a certain percentage of water, vary according to the fluctuations of the water table and daily precipitation. For this study we considered a region contained in the Argentinean Pampas, which in addition to having a low elevation has water tables close to the surface, above 2 m. By means of the simple method implemented, it was possible to note the increase of surface water in the study area on a date when the area suffered a significant flooding. In the interpretation of the results, it is important to have in mind that the Mixed-Water category is more difficult to detect than the Open Water class due to its heterogeneous behaviour.

The use of data from Landsat 8 posed a limitation on this study since scenes are only available each 16 days. In the next stage, adding and working with another satellite system (e.g., Sentinel 2; European Space Agency, 2015) will provide us with a better temporal resolution of scenes and extra data to mitigate the effect of these situations. Moreover, we consider, incorporating data from the Gravity Recovery and Climate Experiment (GRACE) satellite mission, which measures temporal changes in gravity field which is used to compute monthly variations in terrestrial water storage (e.g., Demirel et al., 2019; Strassberg et al., 2007).

ACKNOWLEDGEMENTS This research was supported by Agencia Nacional de Promoción Científica y Tecnológica (ANPCyT), Argentina (PICTs 2017-1406, 2018-02511). The authors would like to express their special thanks to INTA Justiniano Posse Rural Extension Agency for providing the in situ water table level and precipitation data. They also wish to point out that the Landsat data and associated products were courtesy of the U.S. Geological Survey.

REFERENCES

Acharya, T. D., Subedi, A., Lee, D. H., 2018. Evaluation of Water Indices for Surface Water Extraction in a Landsat 8 Scene of Nepal. Sensors, 18(8).

Bollatti, P., Andreucci, A., Escolá, F., 2016. Influencia de los excedentes hídricos en la recarga de los acuíferos libres del sudeste de la provincia de Córdoba. INTA Marcos Juárez. `https://inta.gob.ar/marcosjuarez` (accessed on 25 August 2021).

Boschetti, M., Nutini, F., Manfron, G., Brivio, P. A., Nelson, A., 2014. Comparative analysis of normalised difference spectral indices

derived from MODIS for detecting surface water in flooded rice cropping systems. PloS one, 9(2), e88741.

Capdevila, J., Francisca, F., Zanni, E., 2016. Patologías estructurales asociadas al ascenso de la napa freática en el sureste de la provincia de Córdoba. XXIII Congreso Argentino de Mecánica de Suelos e Ingeniería Geotécnica. Santa Fe, Argentina

Demirel, M. C., Özen, A., Orta, S., Toker, E., Demir, H. K., Ekmekcioğlu, Ö., et al., 2019. Additional value of using satellite-based soil moisture and two sources of groundwater data for hydrological model calibration. Water, 11(10), 2083. European Space Agency, 2015. Sentinel-2 User Handbook. 1–64. Available online at: `https://earth.esa.int/documents/247904/685211/Sentinel-2_User_Handbook`, accessed on 04 October 2021.

Ferral, A., Luccini, E., Aleksinkó, A., Scavuzzo, C. M., 2019. Flooded-area satellite monitoring within a Ramsar wetland Nature Reserve in Argentina. Remote Sensing Applications: Society and Environment, 15, 100230.

Foga, S., Scaramuzza, P. L., Guo, S., Zhu, Z., Dilley Jr, R. D., Beckmann, T., Schmidt, G. L., Dwyer, J. L., Joseph Hughes, M. and Laue, B. 2017. Cloud detection algorithm comparison and validation for operational Landsat data products. Remote Sensing of Environment, 194, 379-390.

Kruse, E., Zimmermann, E., 2002. Hidrogeología de grandes llanuras. Particularidades en la llanura pampeana (Argentina). Workshop Publication on Groundwater and Human Development. La Plata, Argentina.

Li, L., Vrieling, A., Skidmore, A., Wang, T., Muñoz, A.-R.,Turak, E., 2015. Evaluation of MODIS spectral indices for monitoring hydrological dynamics of a small, seasonally-flooded wetland in southern Spain. Wetlands, 35(5), 851–864.

Ma, Z., Liu, Z., Zhao, Y., Zhang, L., Liu, D., Ren, T., Zhang, X.,Li, S., 2020. An Unsupervised Crop Classification Method Based on Principal Components Isometric Binning. ISPRS International Journal of Geo-Information, 9(11), 648.

McFeeters, S. K., 1996. The use of the Normalized Difference Water Index (NDWI) in the delineation of open water features. International Journal of Remote Sensing, 17(7), 1425-1432.

Nosetto, M., Jobbágy, E., Jackson, R., Sznaider, G., 2009. Reciprocal influence of crops and shallow ground water in sandy landscapes of the Inland Pampas. Field Crops Research, 113(2), 138-148.

Ogilvie, A., Belaud, G., Delenne, C., Bailly, J.-S., Bader, J.-C., Oleksiak, A., Ferry, L., Martin, D., 2015. Decadal monitoring of the Niger Inner Delta flood dynamics using MODIS optical data. Journal of Hydrology, 523, 368–383.

Oleksiak, A., 2008. Suivi par télédétection de la dynamique de crue du delta intérieur du Niger pour l'élaboration d'un modèle de fonctionnement hydraulique. Doctoral dissertation, Master 2 professionnel TGAE: Télédétection et Géomatique Appliquées à l'Environnement.

Passucci, V., Carmona, F., Rivas, R. 2017. Identificación de zonas anegadas y no anegadas mediante técnicas de teledetección. Estudios Ambientales, 5.

Pedregosa, F., Varoquaux, G., Gramfort, A., Michel, V.,Thirion, B., Grisel, O., Blondel, M., Prettenhofer, P., Weiss, R., Dubourg, V., Vanderplas, J., Passos, A., Cournapeau, D.,Brucher, M., Perrot, M., Duchesnay, E., 2011. Scikit-learn: Machine Learning in Python.Journal of Machine Learning Research, 12, 2825–2830.

Pekel, J.-F., Cottam, A., Gorelick, N., Belward, A. S., 2016. High-resolution mapping of global surface water and its long-term changes. Nature, 540(7633), 418–422.

Strassberg, G., Scanlon, B. R., Rodell, M., 2007. Comparison of seasonal terrestrial water storage variations from GRACE with groundwater-level measurements from the High Plains Aquifer (USA). Geophysical Research Letters, 34(14).

U.S. Geological Survey, 2016. Landsat—Earth observation satellites (ver. 1.2, April 2020): U.S. Geological Survey Fact Sheet 2015–3081, 4 p.

Vermote, E., Justice, C., Claverie, M., Franch, B., 2016. Preliminary analysis of the performance of the Landsat 8/OLI land surface reflectance product. Remote Sensing of Environment,185, 46-56.

Viglizzo, E. F., Jobbágy, E. G., Carreño, L., Frank, F. C., Aragón, R., De Oro, L., Salvador, V., 2009. The dynamics of cultivation and floods in arable lands of Central Argentina. Hydrology and Earth System Sciences, 13(4), 491-502.

Xu, H., 2006. Modification of normalised difference water index (NDWI) to enhance open water features in remotely sensed imagery. International Journal of Remote Sensing, 27(14), 3025-3033.

Zhou, Y., Dong, J., Xiao, X., Xiao, T., Yang, Z., Zhao, G.,Zou, Z., Qin, Y., 2017. Open Surface Water Mapping Algorithms: A Comparison of Water-Related Spectral Indices and Sensors.Water, 9(4)